Composite Structures, 116:223–234, 2014.

A mixed isostatic 24 dof element for static and buckling analysis of laminated folded plates

E. J. Barbero
West Virginia University, Morgantown USA
and
A. Madeo[1], G. Zagari, R. Zinno, and G. Zucco
University of Calabria, Arcavacata di Rende, CS, Italy

Abstract

A mixed, quadrilateral, 3D plate element is proposed for static linear and buckling analysis of folded laminated composite structures. Numerical results show accuracy, comparing to analytical and numerical references, and convergence rate h^2 measured using an s-norm. These characteristics are due to the self-equilibrated, isostatic state of stress in the element, and to the element kinematics leading to element compliance and compatibility matrix calculations based solely on the interpolation along the element edges. For folded plates, the drilling rotations do not require penalty functions or non-symmetric formulations, thus avoiding spurious energy modes. Buckling analysis is achieved by a corotational formulation, which is possible thanks to the accuracy of rotation approximations. Benchmarking for laminated composite plates includes convergence of displacements and stress-resultants, global error measures, and comparison with literature results.

Keywords

Mixed element; Isostatic; Self-equilibrated; Drilling rotation; Laminated composite; First order shear deformation theory.

1 INTRODUCTION

Folded laminated plates are widely used in the form of structural profiles [1, Fig. 10.1], stiffened panels [1, Section 11.3], cellular structures [2], cold formed steel sections [3], and so on. Open or closed sections composed of flat walls are attractive because they maximize the bending and torsional stiffness for minimum weight and at the same time they take advantage of the high strength of fiber reinforced materials. Using laminated panels affords high flexibility to the design by virtue of the broad range of stiffness and strength that can be imparted to the walls. Ever increasing demands for lightweight structures for transportation vehicles of all kinds requires the use of optimized thin-walled structures for which buckling become the design constraint. Accurate computation of buckling loads, modes, mode interaction [4], and imperfection sensitivity [5, 6] is thus required.

[1]Corresponding author. The final publication is available at http://dx.doi.org/10.1016/j.compstruct.2014.05.003

Since these calculations are computationally intensive, there is significant interest in developing accurate yet economical simulation methods. The use of corotational formulation is quite attractive in this regard because it allows for simple extension to nonlinear analysis of proven, accurate, computationally efficient linear analysis elements.

The aim of this work is to develop and to assess a high performance finite element for linear static and buckling analysis of laminated folded plates with the following features: i) accurate recovery of the solution for very rough meshes, ii) high convergence rate with particular reference to stress recovery, and iii) computational efficiency in terms of total degree of freedom required for the solution

The mixed/hybrid formulation based on Hellinger-Reissner variational formulation has several advantages for the development of high performance finite element [7, 8, 9]. Specifically, it allows both stress and displacements to be represented independently as primary variables, each with its own interpolation functions. It further allows the use of supplementary equilibrium filters [10].

The geometry of folded plates poses additional problems due to the coupling of membrane and bending deformations. Thus, an appropriate handling of drilling rotation is required [9]. Moreover, an accurate recovery of rotational fields is necessary when the geometrical nonlinearity are based on corotational formulation [9]. The use of corotational formulation, decoupling the rigid part of the motion form the elastic response, allows to easily reuse linear finite elements for geometrically non linear analysis, thus avoiding the necessity to setup an ad-hoc interpolation scheme for the nonlinear range.

The literature on the analysis of laminated plate is very rich. A review paper [11] describes the most recent available finite elements based on various laminated theories for buckling and post-buckling, free vibration, dynamics, failure, and damage. Similarly, [12] offers an overview on different strategies for modeling laminated composites plates. Recently proposed elements range from assumed displacements [13, 14], mixed and hybrid formulations [15, 16, 17, 18, 19], mixed interpolation of tensorial components (MITC) [20, 21], NURBS-based isogeometric elements [22], radial point interpolation [23], thickness-stretch deformation elements [24] and zig-zag elements in nonlinear context [25]. Comparison between various laminated composite plate and finite element results are provided in [26].

However, there are only a few finite elements available in the literature that are based on hybrid stress-displacement formulation for the analysis of laminated folded plates. The search for robustness and high performance is ongoing. Recently, Maunder and Izzuddin [27] proposed a hybrid element for folded plates and shells, with particular emphasis on the interpolation along the folded sides, with the objective of obtaining an accurate, robust finite element and computational less expensive solutions.

Publications that describe geometrical nonlinearity with corotational formulation are few and often they are not based on mixed formulation and/or free from using penalty constraints to the handle the drilling rotation (see [28, 29, 30]).

In this sense, the present manuscript is one of the few available in which a simple mixed/hybrid formulation is proposed for the static and buckling analysis of folded laminated folded plates, resulting in a good compromise among simplicity, accuracy, and efficiency.

The starting point is the available linear, mixed formulation element called MISS-4 [31]. The stress resultant interpolation, which accounts for the average distortion of the element, is self-equilibrated and isostatic. Only 18 stress parameters are used into 6 constant, 8 linear, and 4 quadratic stress shape functions. The kinematics uses 6 degrees of freedom (dof) per node for an overall 24 dof. Convergence rate and accuracy is shown in this work to be comparable to that of 48 dof, displacement based elements such as Abaqus S8R.

The performance of the linear element has been shown previously to be very good for the case

of isotropic material, both for the recovery displacements and rotations as well as for evaluation of stress resultants. Numerical results have demonstrated s-norm h^2 convergence rate [32]. In this paper, this is shown to be the case also for laminated folded plates by using numerous and varied examples. Furthermore, the element is free from locking. The element matrices are evaluated analytically along the contour. Moreover, the element uses 6 standard degrees of freedom (dof) per node (3 displacements and 3 rotations), thus allowing for trivial implementation as a user element into commercial codes [31, 7].

The drilling rotations are implemented as per [33, 34], without un-symmetric formulation or penalty constraints [35], allowing for an accurate recovery of drilling rotation field; thus enabling the element to be used for geometrically nonlinear analysis using a corotational formulation [36, 37, 38, 39, 40]. An incompatible cubic mode is used to eliminate the spurious zero energy mode [9].

The novelty of this contribution resides in the incorporation of appropriate kinematics (FSDT) and its corresponding constitutive equation into the hybrid-corotational element described in [31], and more importantly, the assessment of the element performance, for the cases of linear static and buckling analyses, for numerous and practical laminated composite folded plate examples, including comparison with accepted test cases from the literature.

The laminate kinematics has been approximated by first order shear deformation theory (FSDT) [41, 42], which offers a good compromise between simplicity and accuracy in the recovery of displacements, rotations, and stress resultants. Furthermore, the mixed stress-displacement formulation chosen for this work allows for better recovery of stress profiles than displacement-only formulations [43, 44].

Using the corotational formulation, the linear element is here extended for laminated folded plates. Then, numerical comparison is presented to demonstrate the convergence with mesh refinement, mesh distortion, and accuracy for coarse mesh. First, symmetric and unsymmetric laminated plates with cross-ply and angle-ply laminate stacking sequences (LSS) are analyzed for different boundary conditions and thickness-to-span ratios, and the results are compared to analytical solutions [42] and numerical ones available in literature [18]. Particular attention has been given to the convergence of stress results. Then, buckling analysis of a square plate under uniaxial compression (similar to that used by [45]) is presented and the convergence behavior is compared to Abaqus results. Finally, three folded plates are considered, with particular attention to the global convergence for linear static and buckling analysis. Two clamped beams with Ω- and C-shaped sections subjected to shear force, and a clamped box under torsional couple are considered. The discretization error is reported using the s-norm.

The assessment of performance confirms a rate of converge h^2 measured using s-norm with good accuracy also for rough meshes. A similar behavior is shown for buckling analysis. A convergence rate of h^2 is shown in the case of buckling load. Also for this case, the buckling solution is very good for very coarse mesh. The tests confirm that our original aims are satisfied in terms of accuracy and computational efficiency. The accuracy of the proposed element is comparable to that of commercial eight node shell elements [46] but with a significantly lower computational effort. (24 vs. 48 dof).

2 MIXED VARIATIONAL FORMULATION WITH FSDT

The Hellinger-Reissner functional is

$$\Pi = \Phi - W_{ext} \tag{1}$$

where Φ is the mixed strain energy expressed in terms of stress resultants and generalized displacements and W_{ext} is the work done by external loads. Using FSDT, the mixed strain energy of the

plate can written as

$$\Phi[\boldsymbol{t},\boldsymbol{u}] = \int_\Omega \left\{ \boldsymbol{t}^T \boldsymbol{D}\boldsymbol{u} - \frac{1}{2}\boldsymbol{t}^T \boldsymbol{E}^{-1}\boldsymbol{t} \right\} \mathrm{d}\Omega \tag{2}$$
$$\boldsymbol{t} = \begin{bmatrix} \boldsymbol{t}_m \\ \boldsymbol{t}_f \end{bmatrix}, \quad \boldsymbol{u} = \begin{bmatrix} \boldsymbol{u}_m \\ \boldsymbol{u}_f \end{bmatrix}, \quad \boldsymbol{D} = \begin{bmatrix} \boldsymbol{D}_m & \boldsymbol{0} \\ \boldsymbol{0} & \boldsymbol{D}_f \end{bmatrix}$$

where Ω is the two-dimensional domain, $\{x, y, z\}$ is a Cartesian reference system with the z-axis along the thickness direction, vectors $\boldsymbol{t}_m$ and $\boldsymbol{t}_f$ are the membrane stresses resultant and the bending/shear stress resultants, respectively

$$\boldsymbol{t}_m = \begin{bmatrix} N_x \\ N_y \\ N_{xy} \end{bmatrix}, \quad \boldsymbol{t}_f = \begin{bmatrix} \boldsymbol{t}_b \\ \boldsymbol{t}_s \end{bmatrix} \quad \text{with} \quad \boldsymbol{t}_b = \begin{bmatrix} M_x \\ M_y \\ M_{xy} \end{bmatrix} \quad \text{and} \quad \boldsymbol{t}_s = \begin{bmatrix} S_x \\ S_y \end{bmatrix} \tag{3}$$

The vectors $\boldsymbol{u}_m$ and $\boldsymbol{u}_f$ are the in- and out-of-plane generalized displacements

$$\boldsymbol{u}_m = \begin{bmatrix} u_x \\ u_y \end{bmatrix}, \quad \boldsymbol{u}_f = \begin{bmatrix} u_z \\ \varphi_x \\ \varphi_y \end{bmatrix} \tag{4}$$

The differential operators $\boldsymbol{D}_m$ and $\boldsymbol{D}_f$ are defined as

$$\boldsymbol{D}_m = \begin{bmatrix} \partial/\partial x & 0 \\ 0 & \partial/\partial y \\ \partial/\partial y & \partial/\partial x \end{bmatrix}, \quad \boldsymbol{D}_f = \begin{bmatrix} 0 & 0 & -\partial/\partial x \\ 0 & \partial/\partial y & 0 \\ 0 & \partial/\partial x & -\partial/\partial y \\ \partial/\partial x & 0 & 1 \\ \partial/\partial y & -1 & 0 \end{bmatrix} \tag{5}$$

The constitutive matrix for a laminate with n layers can be written as

$$\boldsymbol{E} = \begin{bmatrix} \boldsymbol{E}_m & \boldsymbol{E}_{mb} & \boldsymbol{0} \\ & \boldsymbol{E}_b & \boldsymbol{0} \\ \text{sym.} & & \boldsymbol{E}_s \end{bmatrix} \tag{6}$$

where

$$\begin{aligned} \boldsymbol{E}_m &= \sum_k^n (z_k - z_{k-1}) \boldsymbol{E}_m^{(k)} \\ \boldsymbol{E}_{mb} &= \frac{1}{2} \sum_k^n (z_k^2 - z_{k-1}^2) \boldsymbol{E}_m^{(k)} \\ \boldsymbol{E}_b &= \frac{1}{3} \sum_k^n (z_k^3 - z_{k-1}^3) \boldsymbol{E}_m^{(k)} \\ \boldsymbol{E}_s &= \boldsymbol{\kappa} \odot \sum_k^n (z_k - z_{k-1}) \boldsymbol{E}_s^{(k)} \end{aligned} \tag{7}$$

where z_k, z_{k-1} are the top and bottom coordinates of k-th lamina, respectively, $\boldsymbol{E}_m^{(k)}, \boldsymbol{E}_s^{(k)}$ are the lamina constitutive matrices referring to in-plane and transverse stress/strain, respectively [42] and [1, Eq.(6.16)]. Finally, symbol $\odot$ denotes the component product (.* in [47]) that allows us to introduce different shear correction factors for each component of the $\boldsymbol{E}_s$ matrix [16, 48]

$$\boldsymbol{\kappa} = \begin{bmatrix} \kappa_{11} & \kappa_{12} \\ \kappa_{12} & \kappa_{22} \end{bmatrix} \tag{8}$$

3 MISS-4 ELEMENT

The geometry of the Mixed Isostatic Self-equilibrated Stress (MISS-4) element [31] is described by four nodal coordinates on the plane $Z = 0$ of the global Cartesian system $\{X, Y, Z\}$ and the element connectivity (Fig. 1).

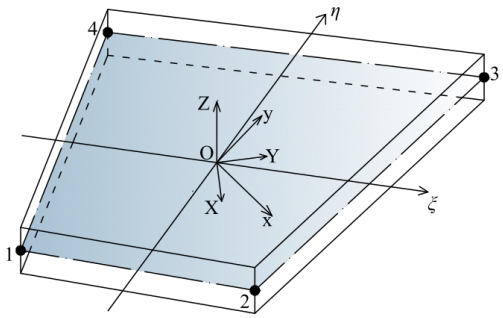

Figure 1: Global, local and internal coordinate systems.

Next, a dimensionless internal system is defined over the element mid surface with $\{\xi, \eta\}$, $-1 \leq \xi \leq 1, -1 \leq \eta \leq 1$, which is implicitly defined by

$$\begin{cases} X = a_0 + a_1\xi + a_2\xi\,\eta + a_3\eta \\ Y = b_0 + b_1\xi + b_2\xi\,\eta + b_3\eta \end{cases} \tag{9}$$

where

$$\begin{bmatrix} a_0 & b_0 \\ a_1 & b_1 \\ a_2 & b_2 \\ a_3 & b_3 \end{bmatrix} = \frac{1}{4}\begin{bmatrix} 1 & 1 & 1 & 1 \\ -1 & 1 & 1 & -1 \\ 1 & -1 & 1 & -1 \\ -1 & -1 & 1 & 1 \end{bmatrix}\begin{bmatrix} X^1 & Y^1 \\ X^2 & Y^2 \\ X^3 & Y^3 \\ X^4 & Y^4 \end{bmatrix} \tag{10}$$

where $\{X^i, Y^i\}$, $i = 1, .., 4$ are the global nodal coordinates.

The third system is a local Cartesian system $\{x, y\}$, defined over the element mid surface, centered and aligned with the element. To define the local system, we introduce the Jacobian matrix $\boldsymbol{J}^G$ and its average $\bar{\boldsymbol{J}}^G$

$$\begin{aligned} \boldsymbol{J}^G &= \begin{bmatrix} X_{,\xi} & X_{,\eta} \\ Y_{,\xi} & Y_{,\eta} \end{bmatrix} = \begin{bmatrix} (a_1 + a_2\eta) & (a_3 + a_2\xi) \\ (b_1 + b_2\eta) & (b_3 + b_2\xi) \end{bmatrix} \\ \bar{\boldsymbol{J}}^G &= \frac{1}{4}\int_{\xi=-1}^{1}\int_{\eta=-1}^{1} \boldsymbol{J}^G\,\mathrm{d}\xi\,\mathrm{d}\eta = \begin{bmatrix} a_1 & a_3 \\ b_1 & b_3 \end{bmatrix} \end{aligned} \tag{11}$$

The average Jacobian $\bar{\boldsymbol{J}}^G$ is decomposed into an orthogonal matrix $\boldsymbol{R}$ and a symmetric matrix $\bar{\boldsymbol{J}}$, so that

$$\begin{aligned} &\bar{\boldsymbol{J}}^G = \boldsymbol{R}\,\bar{\boldsymbol{J}} \\ &\boldsymbol{R} = \begin{bmatrix} \cos\alpha & -\sin\alpha \\ \sin\alpha & \cos\alpha \end{bmatrix}, \quad \alpha = \arctan\left(\frac{a_3 - b_1}{a_1 + b_3}\right), \quad \bar{\boldsymbol{J}} = \begin{bmatrix} a & c \\ c & b \end{bmatrix} \end{aligned} \tag{12}$$

The local Cartesian system $\{x, y\}$ has its origin at the element centroid ($\xi = \eta = 0$) and is rigidly rotated by $\boldsymbol{R}$ with respect to $\{X, Y\}$. The coordinates $\{x, y\}$ are defined according the

transformation

$$\begin{bmatrix} x \\ y \end{bmatrix} = \boldsymbol{R}^T \begin{bmatrix} X - a_0 \\ Y - b_0 \end{bmatrix} \tag{13}$$

The use of a local system $\{x, y\}$ allows us to eliminate the rigid part of the global element distortion, providing a finite element description that is objective with respect to a rigid body motion of the element.

3.1 Assumed stresses

The stresses are assumed to be self equilibrated and isostatic, leading to a minimum set of parameters, which are the 18 components of the vector $\boldsymbol{\beta}_e$. Then, the stress resultants can be written as

$$\boldsymbol{t} = \boldsymbol{B}\boldsymbol{\beta}_e = \begin{bmatrix} \boldsymbol{B}_m & \boldsymbol{0} \\ \boldsymbol{0} & \boldsymbol{B}_f \end{bmatrix} \begin{bmatrix} \boldsymbol{\beta}_m \\ \boldsymbol{\beta}_f \end{bmatrix} \tag{14a}$$

where $\boldsymbol{B}_m$ and $\boldsymbol{B}_f$ are matrices representing the assumed stress modes for the membrane and flexural generalized stresses, respectively, and $\boldsymbol{\beta}_m, \boldsymbol{\beta}_f$ are 9-component vectors representing membrane and flexural effects, respectively. For the membrane stresses, it is assumed that

$$\boldsymbol{B}_m = \begin{bmatrix} 1 & 0 & 0 & y & 0 & x & 0 & y^2 & -2\,a^2\,x\,y \\ 0 & 1 & 0 & 0 & x & 0 & y & -x^2 & 2\,b^2\,x\,y \\ 0 & 0 & 1 & 0 & 0 & -y & -x & 0 & a^2\,y^2 - b^2\,x^2 \end{bmatrix} \tag{14b}$$

For the flexural stress, it is assumed that

$$\boldsymbol{B}_f = \begin{bmatrix} \boldsymbol{B}_b \\ \boldsymbol{B}_s \end{bmatrix} \quad \text{with} \quad \begin{cases} \boldsymbol{B}_b = \begin{bmatrix} 1 & 0 & 0 & x & 0 & y & 0 & x\,y & 0 \\ 0 & 1 & 0 & 0 & x & 0 & y & 0 & x\,y \\ 0 & 0 & 1 & 0 & y\,\bar{c} & x/\bar{c} & 0 & 0 & 0 \end{bmatrix} \\ \boldsymbol{B}_s = \begin{bmatrix} 0 & 0 & 0 & -1 & -\bar{c} & 0 & 0 & -y & 0 \\ 0 & 0 & 0 & 0 & 0 & -1/\bar{c} & -1 & 0 & -x \end{bmatrix} \end{cases} \tag{14c}$$

with $\bar{c} = a^2/b^2$. Both, membrane and flexural stresses are obtained starting from a polynomial expansion in Cartesian coordinates x, y and using Pian's equilibrium filter [31, 9, 10].

3.2 Assumed displacements

The interpolation of the displacement field $\boldsymbol{u}$ is controlled by the 24-component vector $\boldsymbol{u}_e$, collecting displacements and rotations of the four nodes of the element. Since the stress approximation satisfies the equilibrium equation, the internal work can be obtained by integrating on the element contour. Therefore, only contour displacements are needed. The displacement interpolation $\boldsymbol{u}_k$ along element side k is defined as the sum of three contributions

$$\boldsymbol{u}_k[\zeta] = \boldsymbol{u}_{kl}[\zeta] + \boldsymbol{u}_{kq}[\zeta] + \boldsymbol{u}_{kc}[\zeta] \tag{15a}$$

where $-1 \le \zeta \le 1$ is a one-dimensional coordinate along element side k. The first term is a linear expansion

$$\boldsymbol{u}_{kl}[\zeta] = \frac{1}{2}[(1-\zeta)\boldsymbol{u}^i + (1+\zeta)\boldsymbol{u}^j], \quad \begin{cases} \boldsymbol{u}^i = [u_x^i,\, u_y^i,\, u_z^i]^T \\ \boldsymbol{u}^j = [u_x^j,\, u_y^j,\, u_z^j]^T \end{cases} \tag{15b}$$

where superscripts i, j denote the nodes of element side k. The second and third terms correspond to quadratic and cubic expansions for the normal component of the element side displacements

$$\boldsymbol{u}_{kq}[\zeta] = \frac{1}{8} L_k(\zeta^2 - 1) \begin{bmatrix} (\varphi_z^i - \varphi_z^j)\, \boldsymbol{n}_k \\ -(\boldsymbol{\varphi}^i - \boldsymbol{\varphi}^j)^T \cdot \boldsymbol{n}_k \end{bmatrix}, \quad \boldsymbol{u}_{kc}[\zeta] = \frac{1}{4} L_k(\zeta - \zeta^3) \begin{bmatrix} \boldsymbol{n}_k \\ 0 \end{bmatrix} \theta \tag{15c}$$

with

$$\boldsymbol{\varphi}^i = [\varphi_x^i,\, \varphi_y^i]^T \quad , \quad \boldsymbol{\varphi}^j = [\varphi_x^j,\, \varphi_y^j]^T \tag{15d}$$

where $\boldsymbol{n}_k = [n_{kx}, n_{ky}]^T$ is the normal to the element side and L_k is the side length; and θ is the average in-plane distortional rotation, defined as

$$\theta = \frac{1}{4} \sum_{i=1}^{4} \varphi_z^i - \bar{\varphi}_z \tag{15e}$$

with $\bar{\varphi}_z$ the average in-plane rigid rotation of the element

$$\begin{aligned} \bar{\varphi}_z &= \boldsymbol{N}_\theta \boldsymbol{u}_{em} \\ \boldsymbol{N}_\theta &= \frac{1}{4\Omega_e} [-d_{4y}, d_{4x}, 0, -d_{1y}, d_{1x}, 0, -d_{2y}, d_{2x}, 0, -d_{3y}, d_{3x}] \quad ; \quad d_k = \begin{bmatrix} x_j - x_i \\ y_j - y_i \end{bmatrix} \end{aligned} \tag{15f}$$

where Ω_e is the are of the element and $u_{em} = \{u_{xi}, u_{yi}, \varphi_{zi}, \ldots\}^T$ collect membrane displacements at nodes $i = 1 \ldots 4$. The rest of the displacements, $u_{ef} = \{u_{zi}, \varphi_{xi}, \varphi_{yi}, \ldots\}^T$, collect the displacements associated to flexural and intralaminar shear at the nodes. By definition, the linear part $\boldsymbol{u}_{kl}$ and the quadratic part $\boldsymbol{u}_{kq}$ are continuous at the inter-element boundaries. The cubic contribution $\boldsymbol{u}_{kc}$ corresponds to an incompatible mode, which is added to avoid rank defectiveness [9]. Finally, a simple bilinear interpolation for bending rotations is used along the side

$$\boldsymbol{\varphi}_k[\zeta] = \frac{1}{2}[(1-\zeta)\boldsymbol{\varphi}_i + (1+\zeta)\boldsymbol{\varphi}_j], \quad \boldsymbol{\varphi}_k[\zeta] = [\varphi_{kx},\, \varphi_{ky}]^T \tag{15g}$$

3.3 Compliance and compatibility

Introducing assumed stress (14) and assumed displacements (15) into the mixed strain energy (2), the mixed strain energy Φ_e of the element can be defined as follows

$$\Phi_e = \boldsymbol{\beta}_e^T \boldsymbol{Q}_e \boldsymbol{u}_e - \frac{1}{2} \boldsymbol{\beta}_e^T \boldsymbol{H}_e \boldsymbol{\beta}_e \tag{16a}$$

where $\boldsymbol{H}_e$ and $\boldsymbol{Q}_e$ are the element compliance matrix and the compatibility matrix respectively. The compliance matrix can be written as follows

$$\boldsymbol{H}_e = \begin{bmatrix} \boldsymbol{H}_m & \boldsymbol{H}_{mb} \\ sym & \boldsymbol{H}_b + \boldsymbol{H}_s \end{bmatrix} \tag{16b}$$

where

$$\boldsymbol{H}_m = \int_{\Omega_e} \{\boldsymbol{B}_m^T \boldsymbol{E}_m^{-1} \boldsymbol{B}_m\}\, \mathrm{d}\Omega, \quad \boldsymbol{H}_{mb} = \int_{\Omega_e} \{\boldsymbol{B}_m^T \boldsymbol{E}_{mb}^{-1} \boldsymbol{B}_b\}\, \mathrm{d}\Omega \tag{16c}$$

and

$$\boldsymbol{H}_b = \int_{\Omega_e} \{\boldsymbol{B}_b^T \boldsymbol{E}_b^{-1} \boldsymbol{B}_b\}\, \mathrm{d}\Omega, \quad \boldsymbol{H}_s = \int_{\Omega_e} \{\boldsymbol{B}_s^T \boldsymbol{E}_s^{-1} \boldsymbol{B}_s\}\, \mathrm{d}\Omega \tag{16d}$$

Since the compatibility matrix is due to self-equilibrated stress interpolation, and it is evaluated trough analytical contour integration, it can be written as follows

$$\boldsymbol{Q}_e = \begin{bmatrix} \boldsymbol{Q}_m & \boldsymbol{0} \\ \boldsymbol{0} & \boldsymbol{Q}_f \end{bmatrix}, \quad \boldsymbol{Q}_m = \sum_{k=1}^{4} \boldsymbol{Q}_{mk}, \quad \boldsymbol{Q}_f = \sum_{k=1}^{4} \boldsymbol{Q}_{fk} \tag{16e}$$

The matrices $\boldsymbol{Q}_{mk}$ and $\boldsymbol{Q}_{fk}$ are defined as follows

$$\begin{aligned} \boldsymbol{\beta}_m^T \boldsymbol{Q}_{mk} \boldsymbol{u}_{em} &= \int_{-1}^{1} \boldsymbol{t}_m^T[\zeta] \boldsymbol{N}_{mk}^T \boldsymbol{u}_{mk}[\zeta] \, \mathrm{d}\zeta \\ \boldsymbol{\beta}_f^T \boldsymbol{Q}_{fk} \boldsymbol{u}_{ef} &= \int_{-1}^{1} \boldsymbol{t}_f^T[\zeta] \boldsymbol{N}_{fk}^T \boldsymbol{u}_{fk}[\zeta] \, \mathrm{d}\zeta \end{aligned} \tag{16f}$$

where $u_{mk} = [u_{kx}, u_{ky}]^T$ and $u_{fk} = [u_{kz}, \varphi_{kx}, \varphi_{ky}]^T$. Finally, the matrices $\boldsymbol{N}_{mk}, \boldsymbol{N}_{fk}$ split the components of the normal to the element side, as follows

$$\boldsymbol{N}_{mk} = \begin{bmatrix} n_{kx} & 0 & n_{ky} \\ 0 & n_{ky} & n_{kx} \end{bmatrix}, \quad \boldsymbol{N}_{fk} = \begin{bmatrix} 0 & 0 & 0 & n_{kx} & n_{ky} \\ n_{kx} & n_{ky} & 0 & 0 & 0 \\ -n_{ky} & 0 & -n_{kx} & 0 & 0 \end{bmatrix}. \tag{16g}$$

4 NUMERICAL RESULTS

An investigation on the performance of the proposed shell element for linear static and buckling analysis of laminated composite folded plates is presented. First, the static linear analysis of laminated composite plates for different laminate stacking sequences (LSS) and span-to-thickness ratios is performed. Particular attention is given to the point-wise and global convergence of the stress resultant to elucidate the behavior of the element for regular and distorted mesh. Then, buckling of simply supported plates is reported. Buckling modes, loads, and their convergence are reported. Finally, linear static and buckling analysis of three folded, laminated-composite, are reported. The first is a clamped Ω section under shear force. The second is a clamped C shaped section under shear force while the third is a clamped box under torsional couple. Different LSS are considered. Global convergence for linear static analysis and convergence on buckling load, buckling modes and comparison with S8R are given.

4.1 Linear static analysis of laminated plates

The benchmark for static linear analysis is a simply supported square plate of side a (see fig. 2) under uniform distributed load q. The lamina elastic properties are: $E_1 = 25$, $E_2 = 1$, $G_{12} = G_{13} = 0.5$, $G_{23} = 0.2$, $\nu_{12} = 0.25$.

Cross-ply and angle-ply laminates are considered, as follows:

i.. A symmetric cross-ply laminate [0/90/0] with SS1 boundary [49, Section 3.1.3] and shear factors $k_{11} = 235445/404004$, $k_{12} = 0$, $k_{22} = 289/360$ [18];

ii.. An antisymmetric cross-ply laminate [0/90], with SS1 boundary and shear factors $k_{11} = k_{22} = 297680/362481$, $k_{12} = 0$ [18];

iii.. An antisymmetric angle-ply [−45/45] [19];

iv.. An angle-ply [−30/60/ − 60/30], with SS2 boundary condition and shear factors $k_{11} = k_{22} = k_{12} = 5/6$ [19].

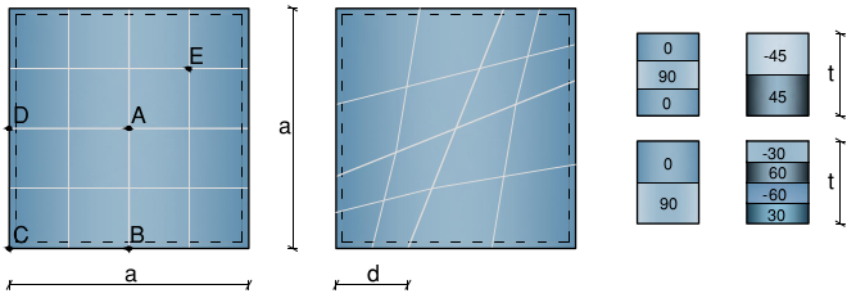

Figure 2: Simply supported square plate. Geometry and mesh.

All results are obtained for side-length/thickness ratio $a/t = 10, 20, 100$. Analytical solutions [42] are used as reference, using the following dimensionless parameters for displacement and stress resultants:

$$\bar{w} = w\frac{100\,E_2}{qt\,(a/t)^4}, \quad \bar{N}_x = N_x\frac{100}{q\,t\,(a/t)^2}, \quad \bar{S}_y = S_y\frac{100}{q\,t\,(a/t)} \tag{17}$$

and

$$\begin{bmatrix} \bar{M}_x \\ \bar{M}_y \\ \bar{M}_{xy} \end{bmatrix} = \frac{100}{q\,t^2\,(a/t)^2}\begin{bmatrix} M_x \\ M_y \\ M_{xy} \end{bmatrix} \tag{18}$$

being w the transversal displacement of the plate.

Point-wise converge for displacements and stress resultant are listed in Tables 1, 2, 3 and 4. The percentage error is defined as

$$error\% = 100 \times \frac{\text{numerical} - \text{analytical}}{\text{analytical}} \tag{19}$$

It can be seen in Tables 1–4 that the convergence to the analytical solution is very fast for all values of span-to-thickness ratio.

Stress resultant convergence are graphed in Figs. 3, 4, 5 and 6. The solid line representing h^2 is shown for reference; where h is the element size of the regular mesh, or span over number of elements per side for irregular meshes. It can be seen that the element displays h^2 convergence for a variety of laminates and span-to-thickness ratios, and that the h^2 convergence is maintained for distorted mesh (Fig. 7).

Point-wise and overall convergence properties are investigated using also distorted mesh with $d = 0.2\,a$ (see Fig. 2). The convergence rate measured using s-norm [32], shows that the rate of convergence is preserved also for distorted mesh (Fig. 7).

The results are compared with the S8R laminated plate elements implemented in the commercial software Abaqus [46, 49] and when available with mixed finite element available in literature [18].

		% error				
a/t	Mesh	$\bar{w}^A$	$\bar{M}_x^E$	$\bar{M}_y^E$	$\bar{M}_{xy}^E$	$\bar{S}_y^E$
10	4x4	3.152	1.197	8.011	21.016	6.552
	8x8	0.745	0.127	1.053	4.986	1.963
	16x16	0.188	-0.019	0.2	1.199	0.506
	32x32	0.051	-0.006	0.043	0.316	0.111
	64x64	0.017	-0.001	0.009	0.095	0.016
20	4x4	3.931	-0.569	9.537	22.012	1.151
	8x8	0.929	-0.174	1.441	4.463	1.402
	16x16	0.226	-0.067	0.315	0.983	0.481
	32x32	0.063	-0.017	0.079	0.227	0.11
	64x64	0.013	-0.003	0.023	0.038	0.015
100	4x4	4.886	-4.264	9.921	24.363	-17.493
	8x8	1.087	-0.338	1.711	4.56	-3.414
	16x16	0.268	-0.086	0.38	0.904	0.015
	32x32	0.06	-0.022	0.101	0.205	0.068
	64x64	0.015	-0.004	0.025	0.041	0.005
		Dimensionless analytical values				
a/t	-	$\bar{w}^A$	$\bar{M}_x^E$	$\bar{M}_y^E$	$\bar{M}_{xy}^E$	$\bar{S}_y^E$
10	-	-1.168	7.016	1.15	-0.317	18.955
20	-	-0.796	7.432	0.888	-0.264	19.976
100	-	-0.671	7.594	0.789	-0.243	20.448

Table 1: Percentage error with respect to the analytical solution values [41] on the transversal displacement at point A, bending moments and shear forces at point E, for regular mesh and span-to-thickness ratios on a simply supported square plate [0/90/0] under uniform distributed load.

		% error			
a/t	Mesh	$\bar{w}^A$	$\bar{M}_x^E$	$\bar{M}_{xy}^E$	$\bar{S}_y^E$
10	4x4	1.553	1.683	7.541	-29.66
	8x8	0.359	0.231	2.138	-16.246
	16x16	0.087	0.032	0.474	-8.555
	32x32	0.021	0.002	0.062	-4.389
	64x64	0.005	-0.005	-0.025	-2.222
20	4x4	1	0.677	9.609	-30.793
	8x8	0.244	0.126	3.044	-16.347
	16x16	0.057	0.008	0.812	-8.538
	32x32	0.006	-0.005	0.171	-4.372
	64x64	0	-0.006	0.006	-2.213
100	4x4	0.724	-0.144	11.321	-32.146
	8x8	0.194	0.008	4.041	-16.747
	16x16	0.041	-0.008	1.257	-8.618
	32x32	0.006	-0.008	0.34	-4.376
	64x64	0	-0.008	0.071	-2.21
		Dimensionless analytical values			
a/t	-	$\bar{w}^A$	$\bar{M}_x^E$	$\bar{M}_{xy}^E$	$\bar{S}_y^E$
10	-	-1.951	6.268	-1.604	-34.703
20	-	-1.759	6.291	-1.577	-34.881
100	-	-1.698	6.301	-1.559	-34.937

Table 2: Percentage error with respect to the analytical solution values [41] on the transversal displacement at point A, bending moments and shear forces at point E, for regular mesh and span-to-thickness ratios on a simply supported square plate [0/90] under uniform distributed load.

		% error				
a/t	Mesh	$\bar{w}^A$	$\bar{M}_x^A$	$\bar{M}_{xy}^C$	$\bar{S}_y^B$	$\bar{N}_x^C$
10	4x4	1.29	9.298	5.699	-30.38	-21.691
	8x8	0.305	2.132	2.862	-16.845	-11.659
	16x16	0.078	0.511	1.109	-8.961	-5.901
	32x32	0.023	0.121	0.363	-4.621	-2.492
	64x64	0.008	0.027	0.098	-2.345	-0.93
20	4x4	0.513	8.206	5.899	-31.78	-18.554
	8x8	0.147	2.054	2.659	-17.046	-6.974
	16x16	0.037	0.497	0.998	-9.026	-3.673
	32x32	0.009	0.117	0.33	-4.656	-1.808
	64x64	0	0.024	0.087	-2.365	-0.761
100	4x4	0.136	7.741	6.274	-33.255	-17.434
	8x8	0.078	2.008	2.885	-17.702	-3.964
	16x16	0.019	0.493	0.991	-9.173	-1.077
	32x32	0	0.12	0.288	-4.679	-0.421
	64x64	0	0.027	0.066	-2.371	-0.234
		Dimensionless analytical values				
a/t	-	$\bar{w}^A$	$\bar{M}_x^A$	$\bar{M}_{xy}^C$	$\bar{S}_y^B$	$\bar{N}_x^C$
10	-	-1.279	3.72	-4.381	-32.788	-0.774
20	-	-1.091	3.745	-4.479	-32.517	-0.697
100	-	-1.031	3.755	-4.552	-32.398	-0.641

Table 3: Percentage error with respect to the analytical solution values [41] on the transversal displacement at point A, bending moments at points A, C, shear forces at point B and membrane stress resultant at point C, for regular mesh and span-to-thickness ratios on a simply supported square plate $[-45/45]$ under uniform distributed load.

		% error			
a/t	Mesh	$\bar{w}^A$	$\bar{M}_x^A$	$\bar{M}_y^A$	$\bar{S}_y^D$
10	4x4	2.818	0.413	2.057	-27.937
	8x8	0.54	-0.211	0.038	-15.242
	16x16	0.097	-0.1	-0.084	-7.994
	32x32	0.011	-0.034	-0.034	-4.096
	64x64	0	-0.014	-0.014	-2.071
20	4x4	2.313	-0.345	1.507	-28.723
	8x8	0.397	-0.32	-0.02	-15.368
	16x16	0.055	-0.121	-0.091	-8.029
	32x32	0	-0.04	-0.036	-4.109
	64x64	0	-0.016	-0.014	-2.08
100	4x4	2.066	-0.465	1.573	-29.419
	8x8	0.329	-0.366	-0.034	-15.88
	16x16	0.045	-0.128	-0.088	-8.1
	32x32	0	-0.042	-0.036	-4.11
	64x64	0	-0.016	-0.016	-2.078
		Dimensionless analytical values			
a/t	-	$\bar{w}^A$	$\bar{M}_x^A$	$\bar{M}_y^A$	$\bar{S}_y^D$
10	-	-0.926	7.126	4.419	-37.18
20	-	-0.731	7.274	4.413	-37.117
100	-	-0.668	7.326	4.412	-37.109

Table 4: Percentage error with respect to the analytical solution values [41] on the transversal displacement at point A, bending moments at point A and shear force at point D, for regular mesh and span-to-thickness ratios on a simply supported square plate $[30/-60/60/-30]$ under uniform distributed load.

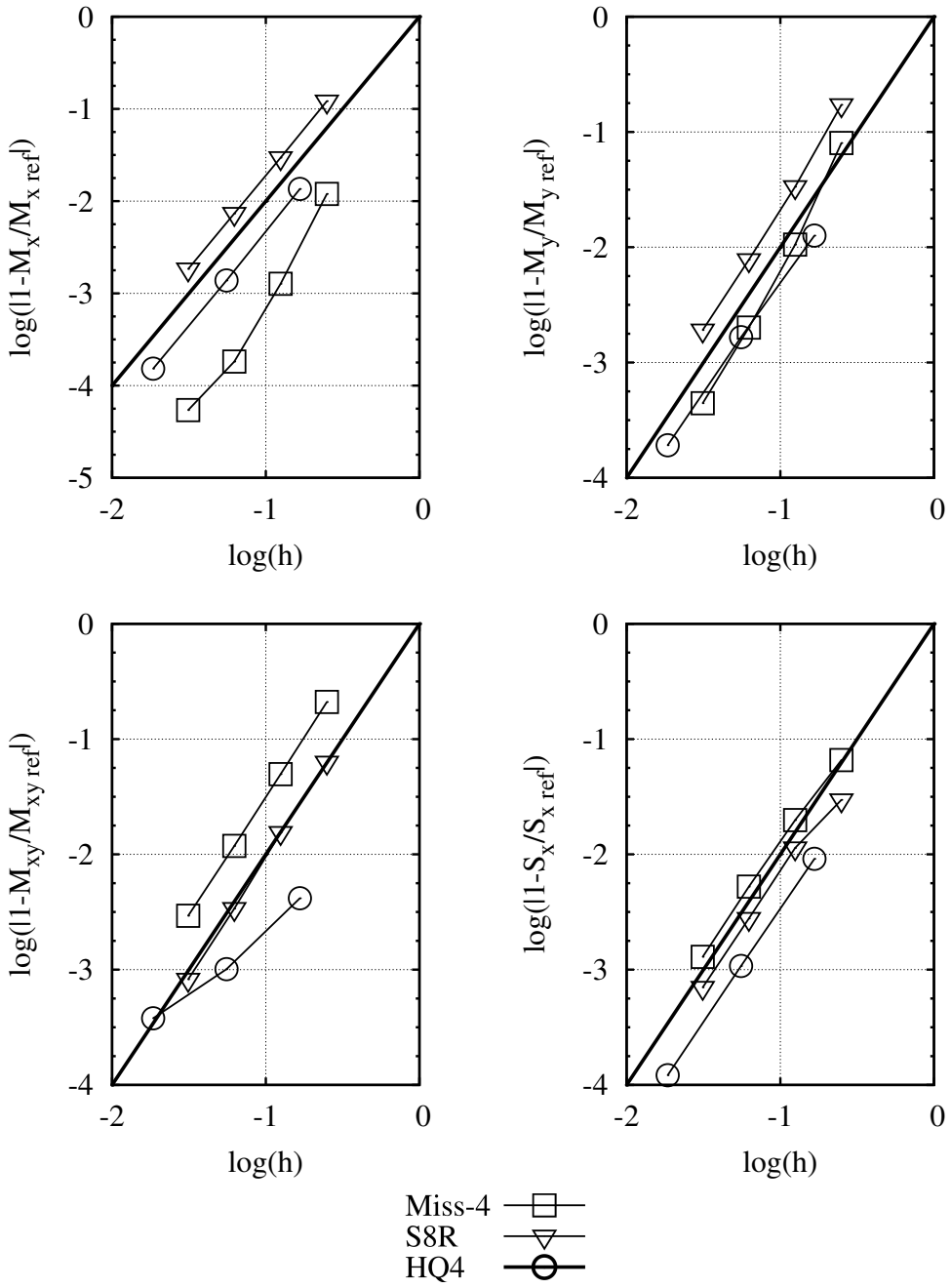

Figure 3: Simply supported square plate [0/90/0]. Convergence of bending moments and shear forces at point E, for regular for various values of span-to-thickness ratio. The solid line represents h^2 (shown for reference). S8R (Abaqus) and HQ4 [18] results are shown for comparison.

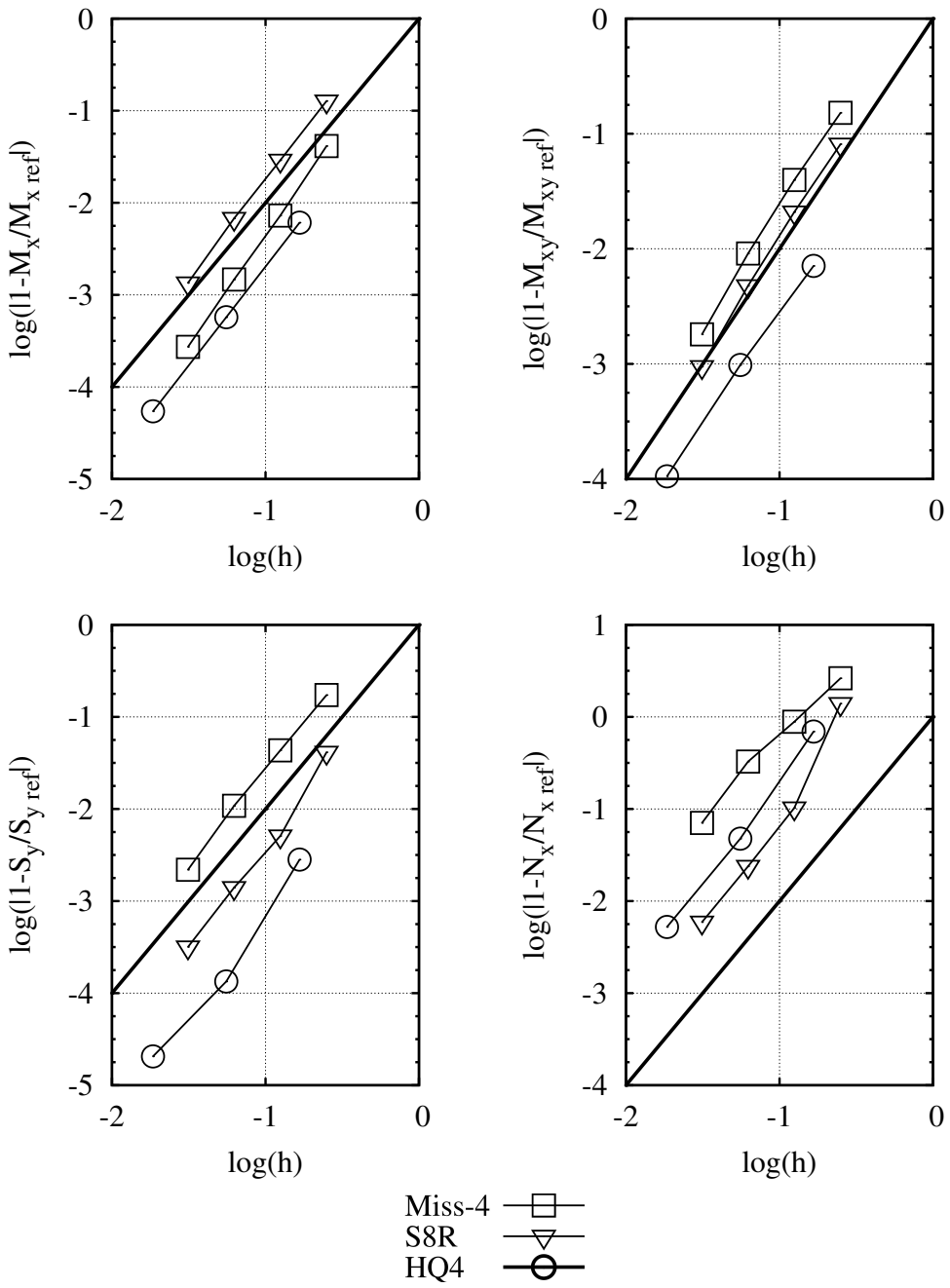

Figure 4: Simply supported square plate [0/90]. Convergence graphs for flexural moments, shear stress resultant, and axial stress resultant at point E for different span-to-thickness ratio using regular mesh. S8R (Abaqus) and HQ4 [18] results are shown for comparison.

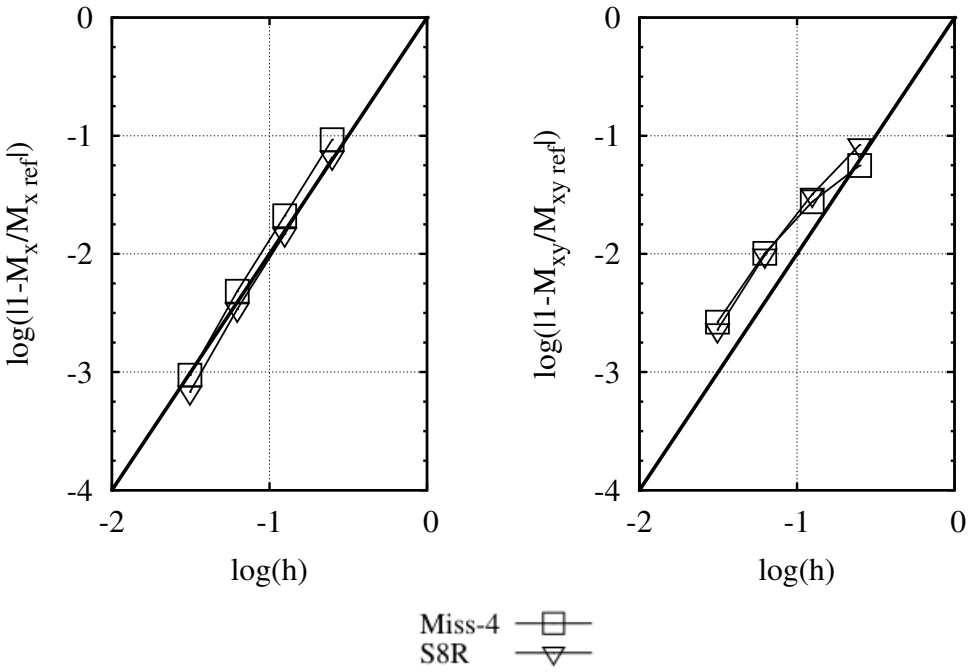

Figure 5: Simply supported square plate [−45/45]. Convergence graphs for flexural moments resultant at points A and C for different span-to-thickness ratios using regular mesh. S8R (Abaqus) and HQ4 [18] results are shown for comparison.

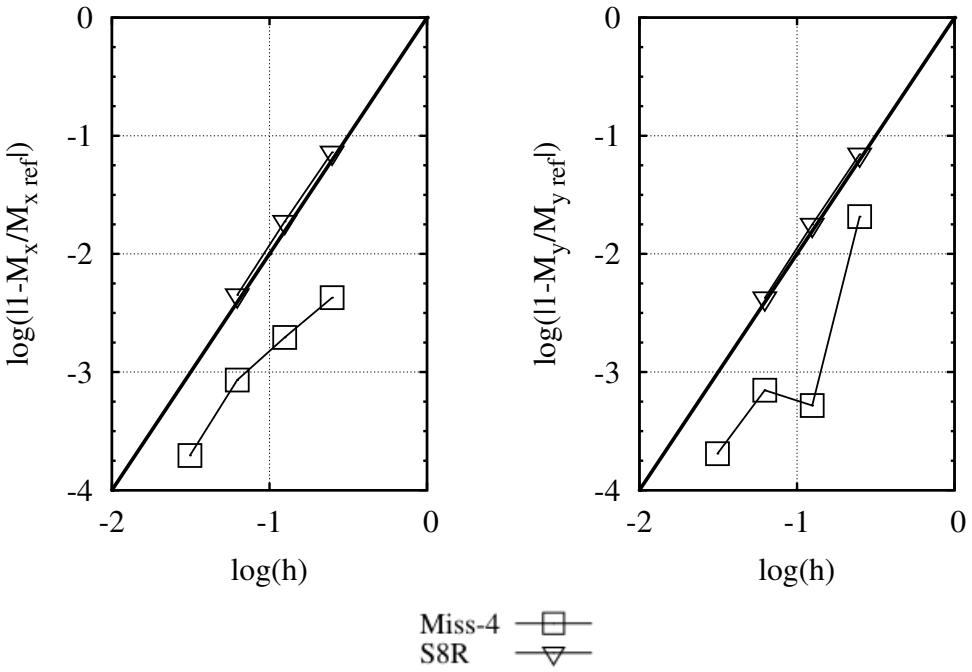

Figure 6: Simply supported square plate $[30/-60/60/-30]$. Convergence graphs for flexural moments resultant at points A for different span-to-thickness ratio using regular mesh. S8R (Abaqus) and HQ4 [18] results are shown for comparison.

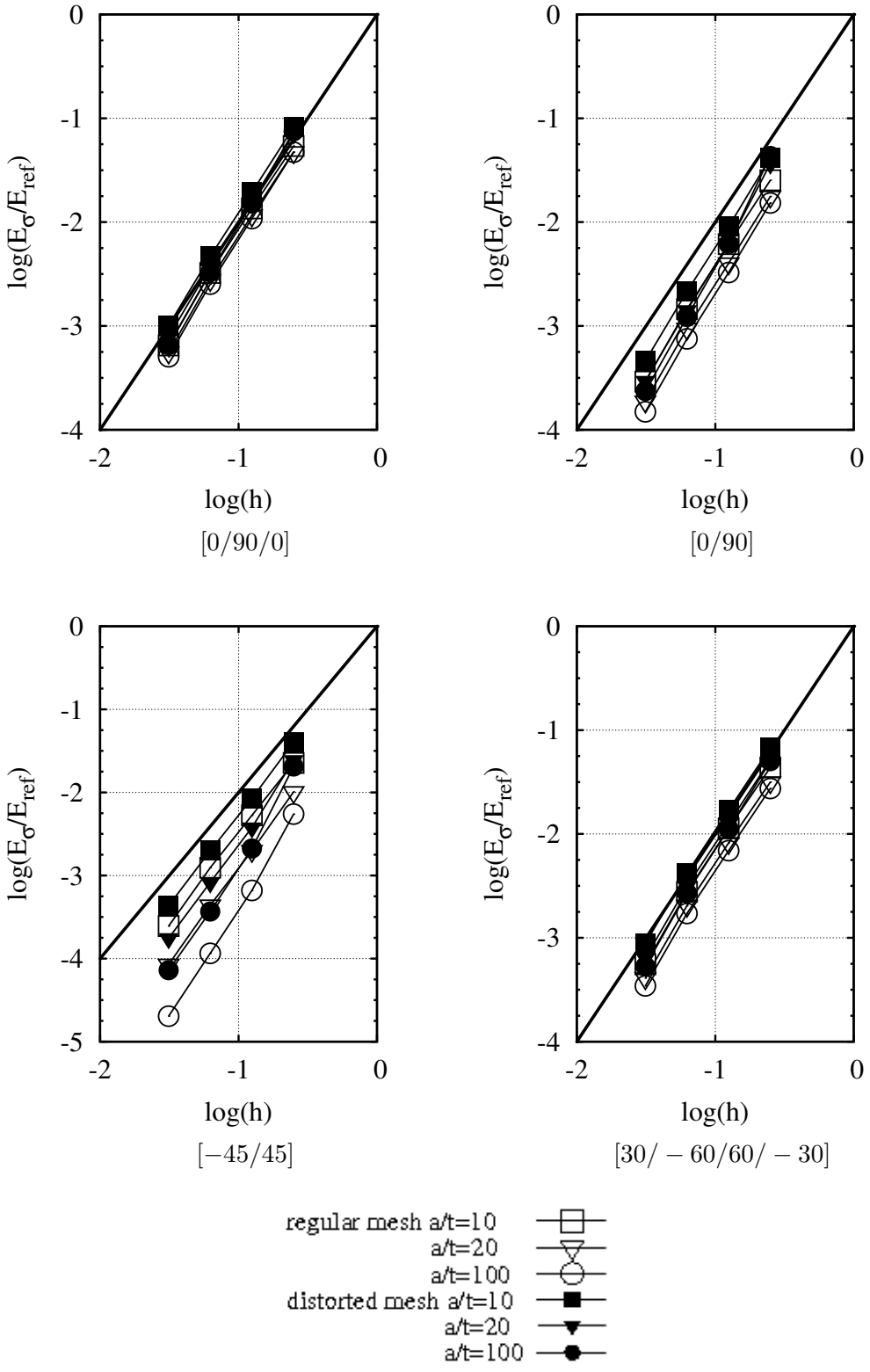

Figure 7: Simply supported square plate for different LSS. Convergence graphs using s-norm, for different span-to-thickness ratio using regular and distorted mesh. E_{ref} calculated with the proposed element, using a very fine mesh.

4.1.1 Buckling analysis of a laminated square plate

The buckling analysis of a laminated square plate ($l \times l \times t$) is presented here. The geometry, material properties, boundary, and load conditions are taken from [45]. The plate is simply supported on its boundary and loaded with a uniform edge pressure λ. The thickness is $t = 1.272\,10^{-4}$ m. The length is $l = 0.508$ m. The LLS is $[0/90/90/0]_S$. The lamina materials properties are $E_1 = 181$ GPa, $E_2 = 10.27$ GPa, $G_{12} = 7.17$ GPa, $\nu_{12} = 0.28$. The critical loads are listed in Table 5 and the buckling modes are shown in Fig. 8. Note that h^2 convergence is achieved for buckling loads (i.e., eigenvalues) as shown in Fig. 9. While the results obtained using the proposed element coincide with those obtained using Abaqus S8R elements when both use a 64x64 mesh, it must be noted that the proposed element has only 24 dof in comparison to 48 dof for S8R.

mesh	λ_1	λ_2	λ_3	λ_4	λ_5	λ_6
4x4	1.757	4.505	11.140	11.852	17.938	19.140
8x8	1.548	3.575	7.083	8.008	10.677	11.827
16x16	1.500	3.365	6.202	7.166	8.9565	10.438
32x32	1.489	3.315	6.006	6.968	8.5765	10.131
64x64	1.486	3.303	5.959	6.911	8.4855	10.057
64x64 (S8R)	1.486	3.299	5.944	6.904	8.460	10.033

Table 5: Square plate $[0/90/90/0]_S$ under uniaxial compression. Convergence of buckling loads with mesh refinement.

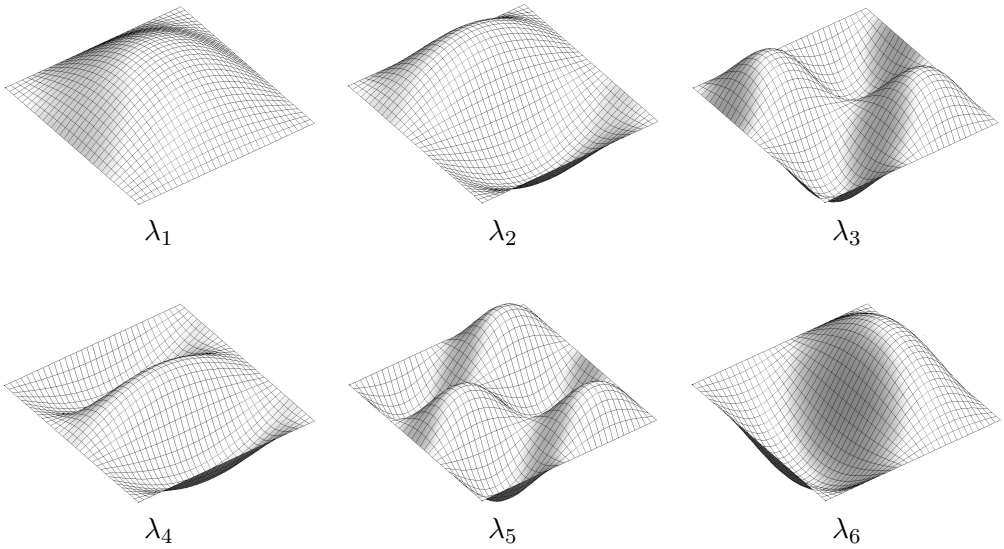

Figure 8: Square plate $[0/90/90/0]_S$ under uniaxial compression. Buckling modes.

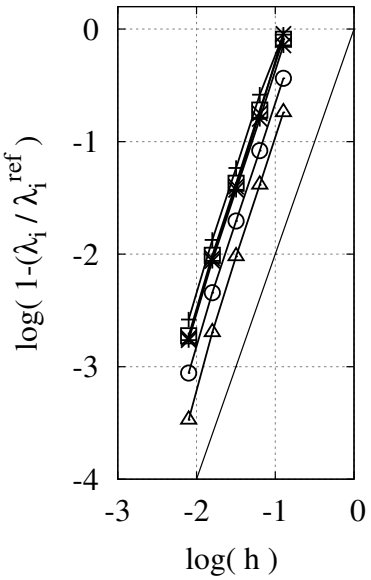

Figure 9: Square plate $[0/90/90/0]_S$ under uniaxial compression. Convergence of buckling loads with mesh refinement. The solid line represents h^2 (for reference).

.

4.2 Linear and buckling analysis of laminated folded plates

The linear static and buckling analysis of three folded plate structures are here presented here. The first is a clamped beam with Ω-section under shear force, the second is a clamped beam with C-section under shear forces, and the third is a clamped box beam subjected to torque. Each folded section is analyzed for various laminate stacking sequences (LSS). For the first section, static linear analysis is performed and the convergence using s-norm is reported. For the second and third sections, buckling convergence as a function of mesh refining is discussed. The predictions are compared with results obtained using element S8R in Abaqus.

4.2.1 Clamped beam with Ω-section under shear force

Linear static analysis of a clamped beam with Ω section is reported here. The geometry is shown in Fig. 10. The length is $l = 100$ mm and the width is $a = 2.5$ mm. Three thickness are considered $a/t = 2, 5/2, 10/3$. The mechanical properties of each lamina are $E_1 = 104$ GPa; $E_2 = 10.3$ GPa; $G = 5.15$ GPa; $\nu_{12} = 0.021$ and two LSS are analyzed, [0/90/0/90] and [0/45/0/45]. A line load $q = 25$ kN/mm is applied. The global convergence using s-norm is reported in Fig. 11 and a rate of convergence h^2 is shown.

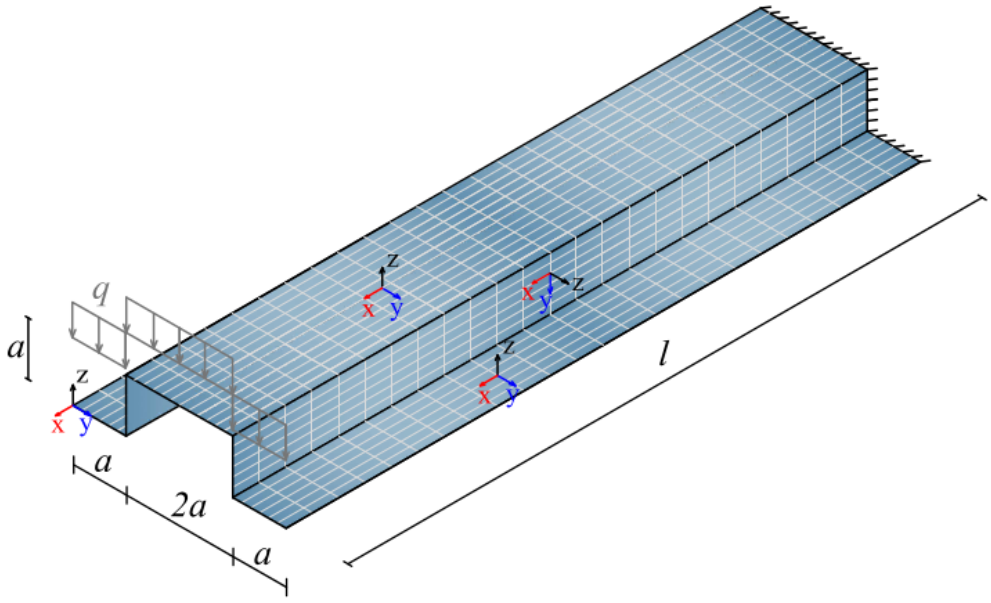

Figure 10: Clamped beam with Ω-section. Geometry, boundary conditions and mesh.

4.2.2 Clamped beam C-section under shear force

The buckling analysis of folded C-section [50] is presented here. The geometrical data (Fig. 12) are $l = 36$ m, $b = 2.025$ m, $a = 6.05$ m and $t = 0.05m$. The concentrated load is $F = 250$ KN. The mechanical properties of each lamina are $E_1 = 30.6$ GPa; $E_2 = 8.7$ GPa; $G_{12} = 3.24$ GPa; $G_{23} = 2.29$ GPa; $\nu_{12} = 0.29$ and two LSS, here called LSS_1 and LSS_2, are analyzed. LSS_1 is shown in Fig. 12 and LSS_2 is a [0/90/0] for all three panels in the C-section. Buckling loads are reported in Table. 6, achieving h^2 convergence, as shown in Fig.13. The corresponding modes are graphed in Fig. 14.

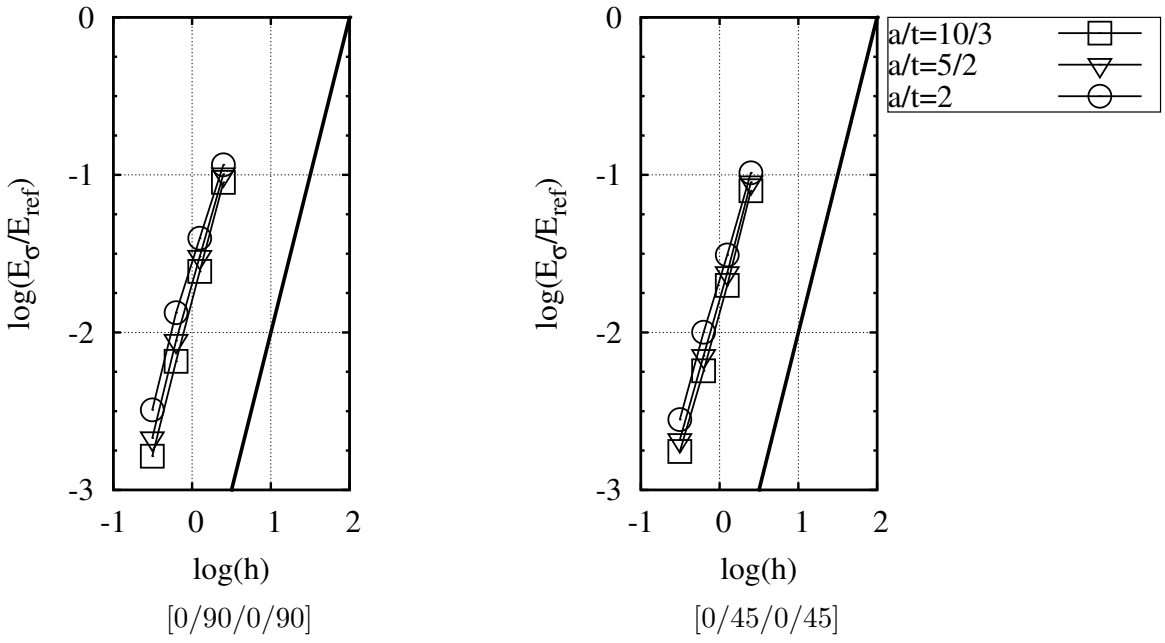

Figure 11: Clamped beam with Ω-section for different LSS. Convergence graphs using s-norm, for different values of a/t using regular mesh. The solid line represents h^2 (shown for reference). E_{ref} calculated with the proposed element, using a very fine mesh.

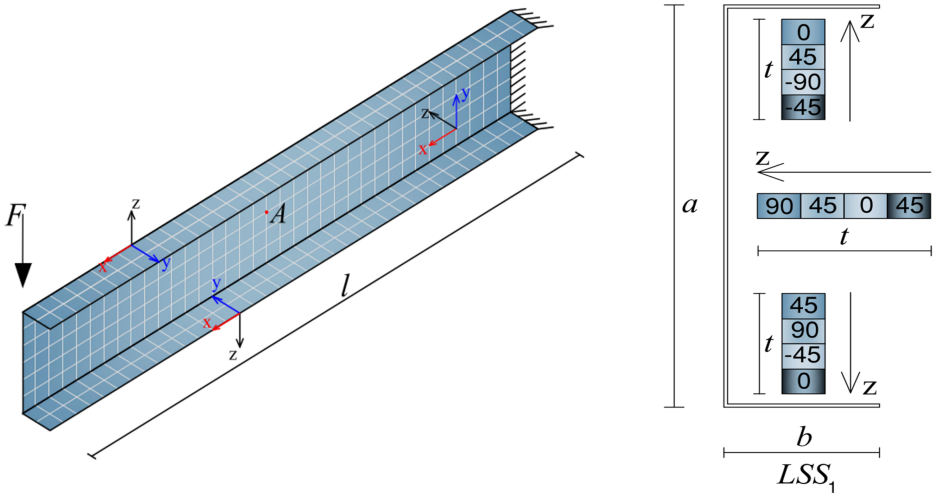

Figure 12: Clamped beam C-section. Geometry, boundary condition and mesh.

	LSS_1				LSS_2			
mesh	λ_1	λ_2	λ_3	λ_4	λ_1	λ_2	λ_3	λ_4
2	1.1209	1.5855	2.1198	2.1807	0.6902	1.6842	2.0256	2.0550
4	1.1010	1.5750	1.6623	1.6963	0.6714	1.5714	1.6667	1.6882
8	1.0952	1.5483	1.5767	1.5859	0.6668	1.5299	1.5836	1.6029
16	1.0935	1.5242	1.5541	1.5760	0.6657	1.5186	1.5633	1.5811
16 (S8R)	1.0736	1.5164	1.5450	1.5919	0.6670	1.5200	1.5865	1.6080

Table 6: Clamped beam C-section for different LSS. Convergence of buckling loads with mesh refinement. The values on the first column refer to the numbers of the element along b.

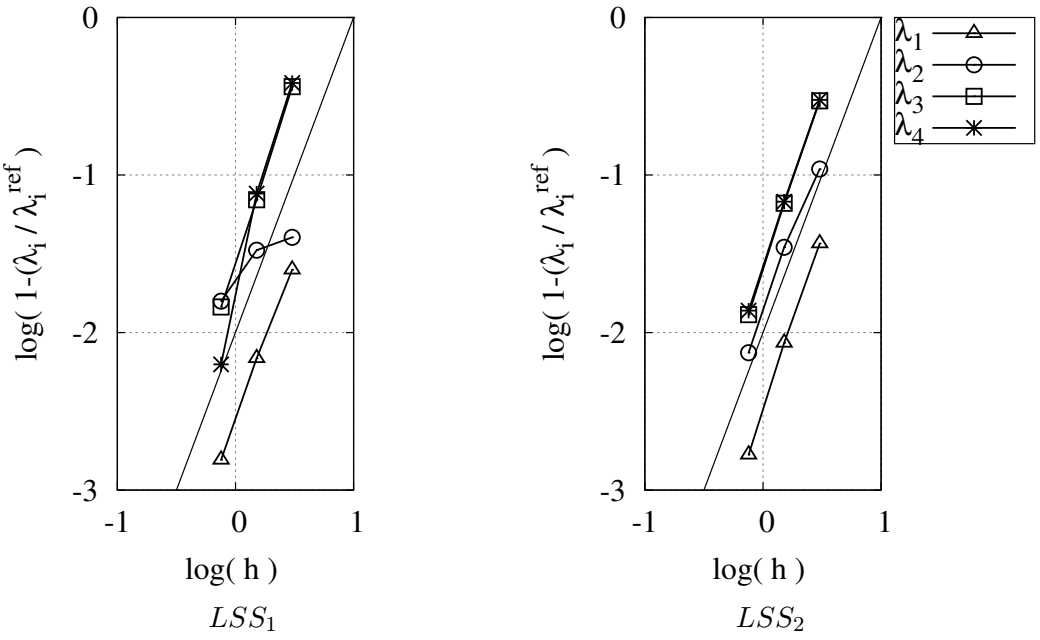

Figure 13: Clamped beam with C-section under shear forces for different LSS. Convergence of buckling loads with mesh refinement. The solid line represents h^2 (for reference). E_{ref} calculated with Abaqus S8R element, using a very fine mesh.

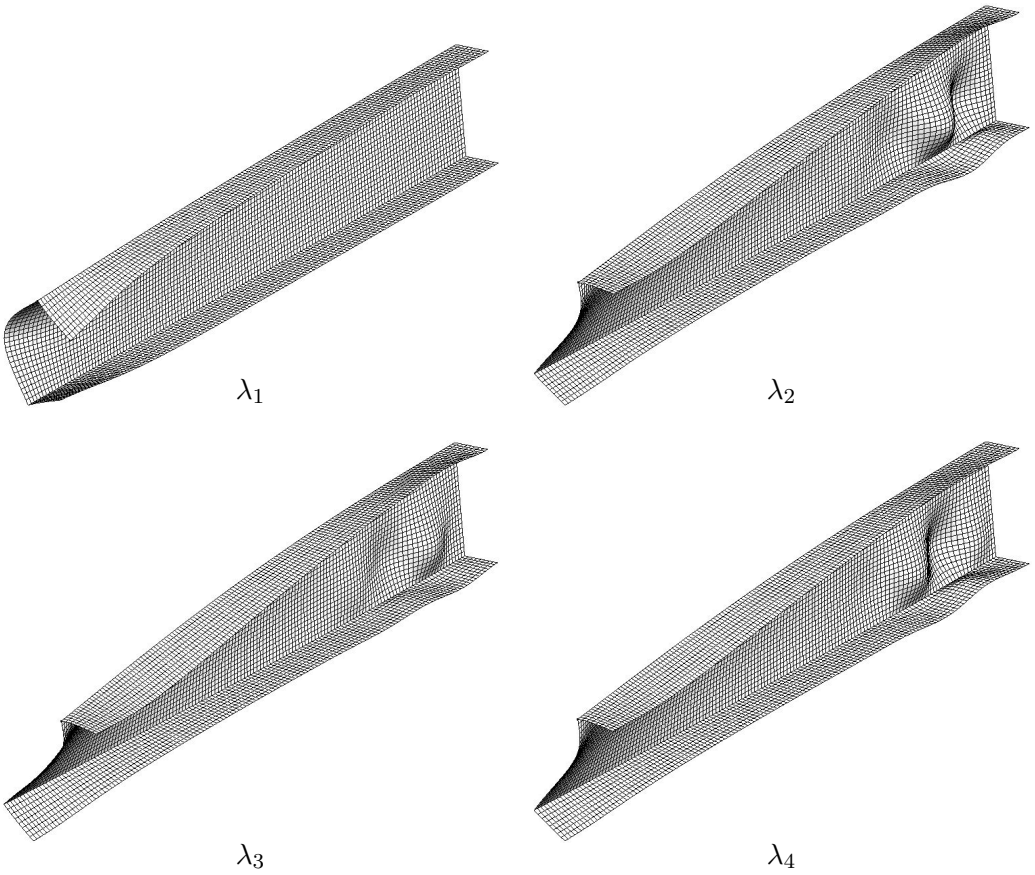

Figure 14: Clamped beam with C-section for LSS=LSS_1. Buckling modes corresponding to buckling loads $\lambda_1..\lambda_4$.

4.2.3 Clamped box under torsional couple

The buckling analysis of a clamped box under torsional couple is presented here. The geometry, boundary conditions, and load are shown in Fig. (15). The geometrical data are $l = 1000$ mm, $a = 100$ mm and $t = 10$ mm. The line load is $q = 25$ kN/mm. Two LLS are considered: $[45/-45/45/-45/45]_s$ and $[15/-15/15/-15/15]_s$. The elastic modula for the lamina are: $E_1 = 104$ GPa; $E_2 = 10.3$ GPa; $G_{12} = 5.15$ GPa and $\nu_{12} = 0.021$.

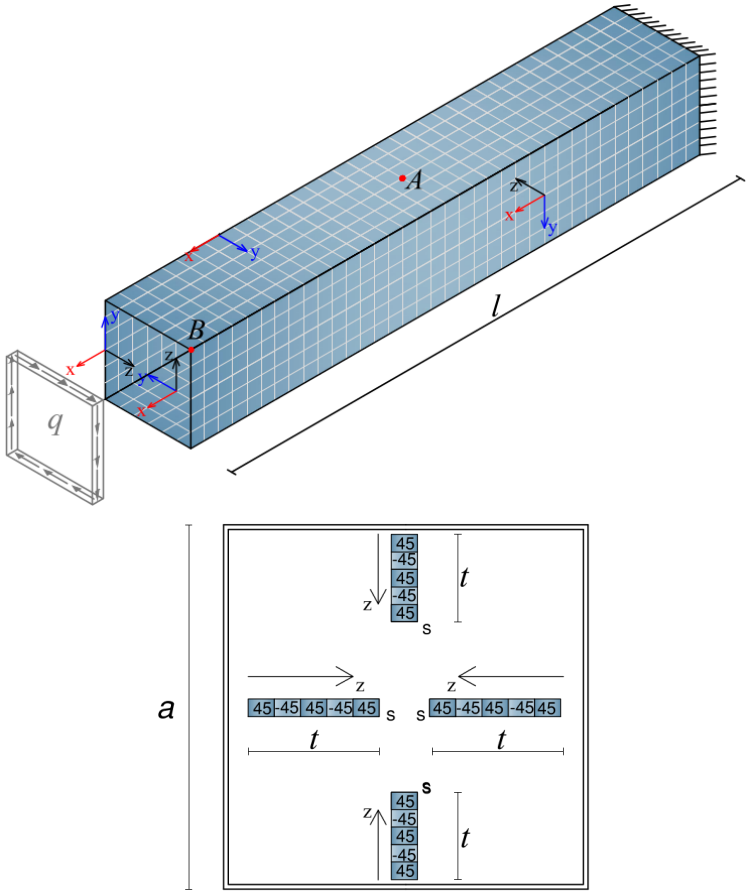

Figure 15: Geometry, boundary conditions, and load for clamped box subjected to torque load.

The lower four buckling modes are listed in Table 7, where comparison with S8R elements have been made, and h^2 convergence is shown in Fig. 16. Finally, buckling modes, for LSS $[45/-45/45/-45/45]_s$, are shown in Fig. 17.

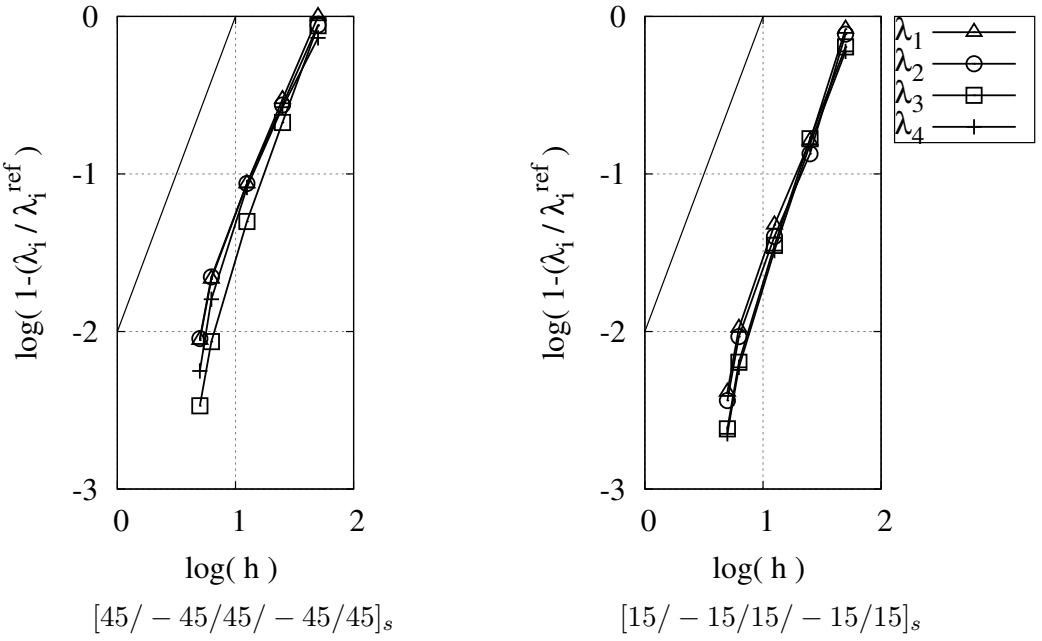

Figure 16: Clamped box under torsional couple for different LSS. Convergence of buckling loads with mesh refinement. The solid line represents h^2 (for reference). E_{ref} calculated with Abaqus S8R element, using a very fine mesh.

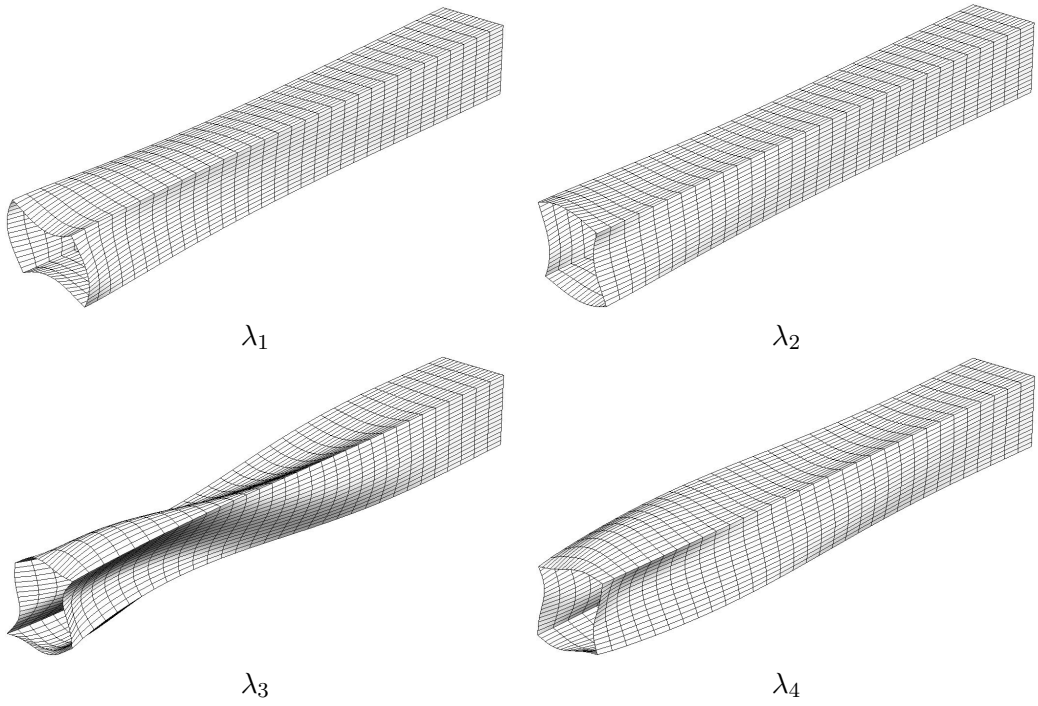

Figure 17: Clamped box under torsional couple with LSS $[45/-45/45/-45/45]_s$. Buckling modes corresponding to buckling loads $\lambda_1 \cdots \lambda_4$.

	$[45/-45/45/-45/45]_s$				$[15/-15/15/-15/15]_s$			
mesh	λ_1	λ_2	λ_3	λ_4	λ_1	λ_2	λ_3	λ_4
2	424.81	453.06	488.72	535.83	195.29	204.22	272.38	278.44
4	241.50	306.71	316.28	391.71	123.95	130.78	193.82	200.86
8	202.34	261.70	273.92	334.97	111.71	119.92	171.88	179.67
16	190.19	246.10	263.15	314.52	107.76	116.36	167.09	175.02
20	187.82	242.93	261.78	311.30	107.08	115.71	166.43	174.38
24	186.18	240.76	260.90	309.56	106.64	115.29	166.03	173.99
24 (S8R)	184.83	242.78	258.47	307.13	106.53	115.63	165.14	173.40

Table 7: Clamped box under torsional couple for different LSS. Convergence of buckling loads with mesh refinement. The values on the first column refer to the numbers of the element along a.

5 CONCLUDING REMARKS

A simple mixed quadrilateral 3D plate finite element with 6 dof/node for linear static and buckling analysis of plate/folded plate has been presented. An assessment of performance is given. In the linear analysis case, numerical results show a global convergence h^2 measured in s-norm for different LSS and thickness-to-span ratios. The point-wise convergence is comparable to that of displacement based elements with higher number of dof, such as S8R. This makes the proposed element particularly suitable for stress resultant recovery in the case of coarse meshes. The use of drilling rotation, within a symmetric formulation and without penalty functions (thus avoiding spurious modes), and accurate evaluation of displacements and rotation, makes the element suitable for folded plate structures and geometrically nonlinear analysis when coupled with a corotational formulation. The same behavior shown in linear analysis of plates is preserved for linear analysis and buckling analysis of folded plates. Not only h^2 convergence is shown for the evaluation of buckling loads but also very low errors are seen, on average, for coarse meshes.

Acknowledgement

The first author acknowledges the support of the Energy Materials Science and Engineering (EMSE) program at West Virginia University. The remaining authors wish to acknowledge the RISPEISE cooperation project for their financial support.

BIBLIOGRAPHY

References

[1] Barbero EJ. Introduction to composite materials design–Second Edition. Boca raton, FL: CRC Press, 2010.

[2] Davalos JF, Chen A, Qiao P. FRP Deck and Steel Girder Bridge Systems: Analysis and Design. Boca Raton, FL: CRC Press, 2013.

[3] Schafer BW. Cold-formed steel structures around the world, Steel Construction 2011; (4) 3.

[4] Barbero EJ. Prediction of Buckling-Mode Interaction in Composite Columns. Mechanics of Composite Materials and Structures, 2000; 7(3):269-284.

[5] Godoy LA. Thin-Walled Structures with Structural Imperfections. NY Elsevier, 1996.

[6] Godoy LA. Theory of Elastic Stability: Analysis and Sensitivity. Philadelphia, PA: Taylor and Francis, 1999.

[7] Bilotta A, Casciaro R. Assumed stress formulation of high order quadrilateral elements with an improved in-plane bending behaviour. Comput Meth Appl Mech Eng, 2002; 191(15-16): 1523-1540.

[8] de Miranda S, Ubertini F. A simple hybrid stress element for shear deformable plates. Int J Numer Methods Eng, 2006; 65(6): 808-833.

[9] Madeo A, Zagari G, Casciaro R. An isostatic quadrilateral membrane finite element with drilling rotations and no spurious modes. Finite Elem Anal Des, 2012; 50: 21-32.

[10] Pian THH, Sumihara K. Rational approach for assumed stress finite elements. Int J Numer Methods Eng, 1984; 20(9): 1685-1695.

[11] Zhang YX, Yang CH. Recent developments in finite element analysis for laminated composite plates. Compos Struct, 2009; 88(1): 147-157.

[12] Khandam R, Noroozi S, Sewell P, Vinney J. The development of laminated composite plate theories: a review. J Mater Sci, 2012; 47: 5901-5910.

[13] Zhang YX, Kim KS. Two simple and efficient displacement-based quadrilateral elements for the analysis of composite laminated plates. Int J Numer Methods Eng, 2004; 61(11): 1771-1796.

[14] Zhang YX, Kim KS. A simple displacement-based 3-node triangular element for linear and geometrically nonlinear analysis of laminated composite plates. Comput Meth Appl Mech Eng, 2005; 194(45): 4607-4632.

[15] Gendy AS, Saleeb AF. Free vibrations and stability analysis of laminated composite plates and shells with hybrid/mixed formulation. Comput Struct, 1997; 63(6): 1149-1163.

[16] Auricchio F, Sacco E. A mixed-enhanced finite-element for the analysis of laminated composite plates. Int J Numer Methods Eng, 1999; 44: 1481-1504.

[17] Auricchio F, Sacco E. Partial-mixed formulation and refined models for the analysis of composite laminates within an FSDT. Compos Struct 1999; 46(2): 103-113.

[18] Daghia F, de Miranda S, Ubertini F, Viola E. A hybrid stress approach for laminated composite plates within the First-order Shear Deformation Theory. Int J Solids Struct, 2008; 45(6): 1766-1787.

[19] Moleiro F, Mota Soares CM, Mota Soares CA, Reddy JN. Mixed least-squares finite element model for the static analysis of laminated composite plates. Comput Struct, 2008; 86(9): 826-838.

[20] Alfano G, Auricchio F, Rosati L, Sacco E. MITC finite elements for laminated composite plates. Int J Numer Methods Eng, 2001; 50(3): 707-738.

[21] Hossain SJ, Sinha PK, Sheikh AH. A finite element formulation for the analysis of laminated composite shells. Comput Struct, 2004; 82(20-21): 1623-1638.

[22] Thai CH, Nguyen-Xuan H, Nguyen-Thanh, Le TH, Nguyen-Thoi T, Rabczuk T. Static, free vibration, and buckling analysis of laminated composite Reissner-Mindlin plates using NURBS-based isogeometric approach. Int J Numer Methods Eng, 2012; 91(6): 571-603.

[23] Liu GR, Zhao X, Dai KY, Zhong ZH, Li GY, Han X. Static and free vibration analysis of laminated composite plates using the conforming radial point interpolation method. Compos Sci Technol, 2008; 68(2): 354-366.

[24] Sgambitterra G, Adumitroaie A, Barbero EJ, Tessler A. A robust three-node shell element for laminated composites with matrix damage. Composites Part B, 2011; 42(1):41-50.

[25] Eby D, Averill RC. Zig-zag sublaminate model for nonlinear analysis of laminated panels. J Aerosp Eng, 2000; 13(3):100-109.

[26] Carrera E, Miglioretti F, Petrolo M. Accuracy of refined finite elements for laminated plate analysis. Compos Struct, 2011; 93(5): 1311-1327.

[27] Maunder EAW, Izzuddin BA. A hybrid equilibrium element for folded plate and shell structures, Int J Numer Methods Eng, 2013; 95:451-477.

[28] Khosravi P, Ganesan R, Sedaghati R. An efficient facet shell element for corotational nonlinear analysis of thin and moderately thick laminated composite structures, Comput Struct, 2008; 86:850-858.

[29] Wang Z, Sun Q. Corotational nonlinear analyses of laminated shell structures using a 4-node quadrilateral flat shell element with drilling stiffness, Acta Mech Sin, 2013,doi 10.1007/s10409-014-0009-x.

[30] Andrade LG, Awruch AM, Morsch IB. Geometrically nonlinear analysis of laminate composite plates and shells using the eight-node hexahedral element with one-point integration, Compos Struct, 2007; 79:571-580.

[31] Madeo A, Zagari G, Casciaro R, de Miranda S. A mixed 4-node 3D plate element based on self-equilibrated isostatic stresses. *accepted for publication Int J Struct Stab Dyn*, 2013.

[32] Hiller JF, Bathe KJ. Measuring convergence of mixed finite element discretizations: an application to shell structures. Comput Structs, 2003; 81(8): 639-654.

[33] Allman DJ. A compatible triangular element including vertex rotations for plane elasticity analysis. Comput Struct, 1984; 19(1-2): 1-8.

[34] Allman DJ. A quadrilateral fiite element including vertex rotations for plane elasticity analysis. Int J. Numer Methods Eng, 1988; 26(3): 717-730.

[35] Hughes T, Brezzi F. On drilling degrees of freedom. Comput Methods Appl Mech Eng, 1989; 72(1): 105-121.

[36] Garcea G, Madeo A, Zagari G, Casciaro R. Asymptotic post-buckling FEM analysis using corotational formulation. Int J Solids Struct, 2009; 46(2): 377-397.

[37] Garcea G, Madeo A, Casciaro R. The implicit corotational method and its use in the derivation of nonlinear structural models for beams and plates. J Mech Mat Struct, 2012; 7(6): 509-538.

[38] Garcea G, Madeo A, Casciaro R. Nonlinear FEM analysis for beams and plate assemblages based on the implicit corotational method. J Mech Mat Struct, 2012; 7(6): 539-574.

[39] Zagari G, Madeo A, Casciaro R, de Miranda S, Ubertini F. Koiter analysis of folded structures using a corotational approach. Int J Solids Struct, 2013; 50(1): 755-765.

[40] Barbero EJ, Madeo A, Zagari G, Zinno R, Zucco G. Koiter asymptotic analysis of folded laminated composite plates. *accepted for publication Composites Part B*, 2014.

[41] Reddy JN. Mechanics of Laminated Composite Plates and Shells - Theory and Analysis. Boca Raton: CRC Press, 1997.

[42] Reddy JN. Mechanics of Laminated Composite Plates and Shells - Theory and Analysis Boca Raton: CRC Press, 2004.

[43] Benedetti A, de Miranda S, Ubertini F. A posteriori error estimation based on the superconvergent Recovery by Compatibility in Patches. Int J Numer Methods Eng, 2006; 67: 108-131.

[44] de Miranda S, Patruno L, Ubertini F. Transverse stress profiles reconstruction for finite element analysis of laminated plates. Compos Struct, 2012; 94(9): 2706-2715.

[45] Raju G, Wu Z, Weaver PM. Postbuckling analysis of variable angle tow plates using differential quadrature method. Compos Struct, 2013; 106: 74-84.

[46] Hibbitt, Karlsson, and Sorensson. Abaqus theory manual, version 6.8. Dassault, 2009.

[47] MATLAB. The Mathworks. Boston, MA, 2013.

[48] Laitinen M, Lahtinen H, Sjölind S G. Transverse shear correction factors for laminates in cylindrical bending. Commun Numer Methods in Eng, 1995; 11(1): 41-47.

[49] Barbero EJ. Finite Element Analysis of Composite Materials using Abaqus. CRC Press, 2013.

[50] Lindgaard E, Lund E. Nonlinear buckling optimization of composite structures. Comput Meth Appl Mech Eng, 2010; 199(37-40): 2319-2330.